Endocytic Sorting of Lipid Analogues Differing Solely in the Chemistry of Their Hydrophobic Tails

Sushmita Mukherjee, Thwe Thwe Soe, and Frederick R. Maxfield

Department of Biochemistry, Weill Medical College of Cornell University, New York 10021

Abstract. To understand the mechanisms for endocytic sorting of lipids, we investigated the trafficking of three lipid-mimetic dialkylindocarbocyanine (DiI) derivatives, $DiIC_{16}(3)$ (1,1′-dihexadecyl-3,3,3′,3′-tetramethylindocarbocyanine perchlorate), $DiIC_{12}(3)$ (1,1′-didodecyl-3,3,3′,3′-tetramethylindocarbocyanine perchlorate), and *FAST* DiI (1,1′-dilinoleyl-3,3,3′,3′-tetramethylindocarbocyanine perchlorate), in CHO cells by quantitative fluorescence microscopy. All three DiIs have the same head group, but differ in their alkyl tail length or unsaturation; these differences are expected to affect their distribution in membrane domains of varying fluidity or curvature. All three DiIs initially enter sorting endosomes containing endocytosed transferrin. $DiIC_{16}(3)$, with two long 16-carbon saturated tails is then delivered to late endosomes, whereas *FAST* DiI, with two cis double bonds in each tail, and $DiIC_{12}(3)$, with saturated but shorter (12-carbon) tails, are mainly found in the endocytic recycling compartment. We also find that $DiOC_{16}(3)$ (3,3′-dihexadecyloxacarbocyanine perchlorate) and *FAST* DiO (3,3′-dilinoleyloxacarbocyanine perchlorate) behave similarly to their DiI counterparts. Furthermore, whereas a phosphatidylcholine analogue with a BODIPY (4,4-difluoro-4-bora-3a,4a-diaza-s-indacene) fluorophore attached at the end of a 5-carbon acyl chain is delivered efficiently to the endocytic recycling compartment, a significant fraction of another derivative with BODIPY attached to a 12-carbon acyl chain entered late endosomes. Our results thus suggest that endocytic organelles can sort membrane components efficiently based on their preference for association with domains of varying characteristics.

Key words: endocytosis • lipid • dialkylindocarbocyanine • membrane domain • membrane curvature

MAMMALIAN cells internalize membrane components and fluid by an assortment of mechanisms that deliver contents to peripherally distributed tubulovesicular sorting endosomes. From the sorting endosomes, most membrane-bound molecules enter the endocytic recycling pathway, while most of the volume gets delivered to late endosomes/lysosomes (Mukherjee et al., 1997). It has been shown that efficient recycling of most membrane-bound molecules does not require any specific signal(s) (Dunn et al., 1989; Mayor et al., 1993).

Although most membrane proteins are efficiently recycled back to the cell surface, some are preferentially retained in the sorting endosomes and are thereby targeted to the late endosomal pathway. Specific amino acid sequences in the cytoplasmic domains of cation-independent mannose-6-phosphate receptor (Johnson and Kornfeld, 1992) and signaling receptors such as the epidermal growth factor receptor (Opresko et al., 1995) have been proposed to mediate their late endosomal targeting. While several lipid analogues with one very short acyl chain {e.g., C_6-NBD-SM [*N*-((6-(7-nitrobenz-2-oxa-1,3-diazol-4-yl)amino)hexanoyl) sphingosyl phosphocholine]} are recycled with an efficiency of 95% or higher (Koval and Pagano, 1989; Mayor et al., 1993), others containing long saturated chains including rhodamine-labeled phosphatidylethanolamine and some glycosphingolipids are delivered predominantly to the late endocytic structures (Kok et al., 1990, 1991; Sandhoff and Klein, 1994). However, the sites of lipid sorting in the endocytic pathway have not been identified, and the efficiency of these sorting processes has not been investigated.

Targeted trafficking of lipids might be due to variations in intrinsic physical properties such as the length and degree of unsaturation of their acyl chains. A consequence of such variation would be differential partitioning preference of these lipids or lipid analogues in coexisting lateral membrane domains of varying composition and motional characteristics ("fluidity" differences). While the lipids with long and saturated acyl chains (such that the length of the acyl chains would roughly match the hydrophobic thick-

Address correspondence to Frederick R. Maxfield, Department of Biochemistry, Weill Medical College of Cornell University, 1300 York Avenue, New York, NY 10021. Tel.: (212) 746-6405. Fax: (212) 746-8875. E-mail: frmaxfie@mail.med.cornell.edu

ness of the surrounding bilayer) will preferentially partition into more rigid or ordered domains, those with short or unsaturated tails would prefer to enter more fluid regions of the bilayer.

Recent studies strongly suggest that the plasma membrane and the membranes of internal organelles of mammalian cells are not in a homogeneous "fluid" state (Brown and London, 1997). While the size, shape, and precise motional properties of the lateral domains are not yet clear, the presence of these domains is likely (Friedrichson and Kurzchalia, 1998; Varma and Mayor, 1998). Glycolipid- and cholesterol-enriched domains have also been proposed to play a role in biosynthetic protein and lipid sorting (Simons and Ikonen, 1997). Furthermore, recent experiments with BODIPY (4,4-difluoro-4-bora-3a,4a-diaza-s-indacene)-labeled lipid analogues indicate that a redistribution of lipids occurs at the plasma membrane or in the forming endosomes within seconds after the initiation of endocytosis (Chen et al., 1997).

The shape of lipids is another characteristic that could cause partitioning into membrane regions of varying curvatures and thereby result in differential trafficking. Indeed, several long saturated chain glycosphingolipids have been found to concentrate in the inner involutions of multivesicular bodies by electron microscopy (Sandhoff and Klein, 1994). Recently, such inward invaginations have been shown to be enriched in a unique lipid, lysobisphosphatidic acid (Kobayashi et al., 1998). It is thus possible that such invaginations, with a curvature opposite to the emanating tubules, may represent a specialized domain that enhances the segregation of some membrane components from the recycling pathway.

Rationale for Choosing the Model Lipids for the Present Study

To determine whether properties of the hydrocarbon tail could efficiently target lipids after internalization, we used the dialkylindocarbocyanine (DiI)[1] series of lipid analogues. These analogues have varying propensities to partition into coexisting lateral membrane domains of varying fluidity and have different relative head group to tail cross-sectional areas resulting in varying overall shapes (approximated as cone, cylinder, or inverted cone). The DiI analogues are composed of an indocarbocyanine head group and two hydrophobic alkyl chains (Fig. 1), which impart to them an overall amphiphilic character (Sims et al., 1974; Haugland, 1996) and allow them to insert into the membrane with their head groups roughly normal to the plane of the bilayer (Axelrod, 1979) in a manner analogous to naturally occurring lipids. The relatively long hydrophobic alkyl chains result in their strong association with the host plasma membrane such that once inserted, they traffic as an integral part of it. Since the DiI derivatives are not naturally occurring lipids, they are not subject to intracellular metabolic turnover.

As shown in Fig. 1, two of the analogues we used contain saturated alkyl chains. $DiIC_{16}(3)$ (1,1′-dihexadecyl-3,3,3′,3′-tetramethylindocarbocyanine perchlorate) has tails with 16 carbons each, whereas $DiIC_{12}(3)$ (1,1′-didodecyl-3,3,3′,3′-tetramethylindocarbocyanine perchlorate) has 12 carbon chains. The differential partitioning preferences of C_nDiIs into domains of varying motional characteristics have been investigated in model membrane systems. In systems with coexisting gel and fluid phases, an approximate match of the probe alkyl chain length with those of the host lipid acyl chains led to a preferential partitioning of the probe into gel phases (Klausner and Wolf, 1980; Spink et al., 1990). The alkyl chain length of $DiIC_{16}(3)$ approximately matches those most prevalent in the lipids of various CHO cell lines (Callaghan et al., 1992; Mackinnon et al., 1992). Thus, in CHO cell membranes, $DiIC_{16}(3)$ would be expected to preferentially partition into more rigid (or highly ordered) domains, whereas $DiIC_{12}(3)$ would enter more fluid domains. The other lipid analogue used in this study, *FAST* DiI (1,1′-dilinoleyl-3,3,3′,3′-tetramethylindocarbocyanine perchlorate), has two 18-carbon chains with two cis double bonds in each chain. Lipids with unsaturated tails preferentially enter fluid domains in model membranes containing coexisting gel and fluid phases (Mouritsen and Jorgensen, 1995).

In rat basophil leukemia (RBL) cells, preferential segregation of $DiIC_{16}(3)$ into specific lateral domains containing aggregated immunoglobulin E receptors has been observed (Thomas et al., 1994). Furthermore, during phagocytosis of 6-μm beads, RBL cells specifically exclude $DiIC_{16}(3)$ but not *FAST* DiI from the forming phagosomes (Pierini et al., 1996).

In addition, the overall shapes of the different DiI derivatives used in this study are quite different, which, in turn, would mean that they would have differential partitioning preferences into membrane regions of varying curvatures (Cullis and de Kruijff, 1979; Gennis, 1989). Both $DiIC_{16}(3)$ and $DiIC_{12}(3)$ have a head group cross-sectional area that is larger than the alkyl chains (provided the chains are stretched out all-trans). They would thus exhibit an inverted cone shape and preferentially partition into membrane regions with a convex curvature. *FAST* DiI has a cylindrical or cone shape by virtue of the cis double bonds and would be preferentially accommodated in membranes of concave curvature. Thus, the set of DiI probes chosen for the present study are ideally suited to address the role of membrane domains in intracellular sorting since they vary in both their fluidity and curvature preferences.

As seen in Fig. 1, the DiO derivatives are identical to their DiI counterparts except that the head groups of DiO contain an oxygen atom as part of the heterocyclic ring system, instead of a carbon atom attached to two methyl groups in DiI (Haugland, 1996). It is thus likely that the DiI and DiO head groups would interact differently with neighboring lipids and/or proteins. Thus, if both DiI and DiO derivatives with the same alkyl chain chemistry traffic identically in CHO cells, it would reinforce the argument that the alkyl chain properties are important in trafficking.

To test a larger variation in head groups, we used phosphatidylcholine derivatives (Fig. 1) that have a zwitterionic head group, unlike the anionic DiI and DiO head groups (Haugland, 1996). One long 16-carbon acyl chain ensured stable incorporation into the membrane bilayer. We used BODIPY FL lipid analogues since the fluoro-

1. *Abbreviations used in this paper:* DiI, dialkylindocarbocyanine; ERC, endocytic recycling compartment; GPI, glycosylphosphatidylinositol; OG, Oregon green–labeled transferrin; Tf, transferrin.

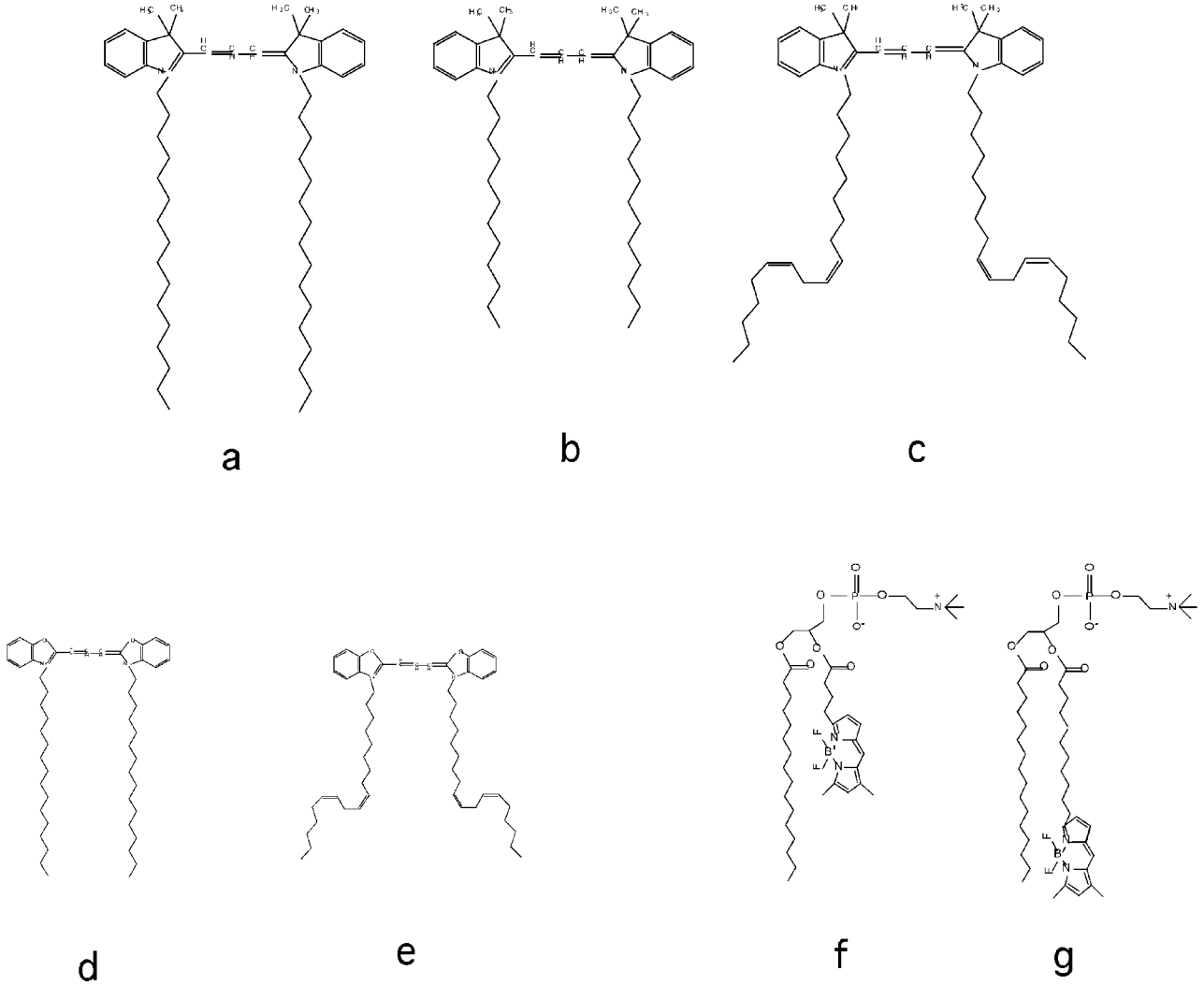

Figure 1. Chemical structures of the lipid analogues used in this study: (a) $DiIC_{16}(3)$, (b) $DiIC_{12}(3)$, (c) *FAST* DiI, (d) $DiOC_{16}(3)$, (e) *FAST* DiO, (f) BODIPY FL C_5-HPC, and (g) BODIPY FL C_{12}-HPC. In the nomenclature, the subscripted numbers refer to the length of the alkyl chains, while the numbers in the parentheses refer to the number of carbons bridging the two indocarbocyanine rings that constitute the head group.

phore has been reported to localize to the membrane interior in a manner roughly normal to the plane of the bilayer (Johnson et al., 1991; Haugland, 1996), whereas in NBD lipid analogues the fluorophore loops back toward the hydrophilic interface (Chattopadhyay and London, 1987). Furthermore, given the size of the BODIPY FL fluorophore, it is expected that incorporating it at the end of a 12-carbon acyl chain would result in a derivatized acyl chain that would roughly span the thickness of one membrane leaflet in a CHO cell. BODIPY FL C_{12}-HPC [2-(BODIPY-3-dodecanoyl)-1-hexadecanoyl-*sn*-glycero-3-phosphocholine] would thus be somewhat similar to the $DiIC_{16}(3)$ or $DiOC_{16}(3)$ in terms of the properties of the hydrophobic tail. BODIPY FL C_5-HPC [2-(BODIPY-3-pentanoyl)-1-hexadecanoyl-*sn*-glycero-3-phosphocholine] would, on the other hand, be expected to more closely mimic $DiIC_{12}(3)$.

Materials and Methods

Materials

All fluorescence probes were obtained from Molecular Probes Inc. The purity of the lipid analogues was checked by thin layer chromatography using chloroform/methanol/water (65:35:5 vol/vol) as the solvent system. Labeled dextran was dissolved in PBS, pH ~7.4, and was extensively dialyzed before use to remove any unconjugated dye. Cy3 was obtained as a protein conjugation kit from Amersham Life Sciences.

Human transferrin (Tf) was obtained from Sigma Chemical Co. It was then iron loaded and passed through a Sephacryl S-300 gel filtration system as previously described (Yamashiro et al., 1984). Succinimidyl ester of Oregon green, Alexa 488, and Cy3 were then separately conjugated to the iron-loaded Tf following the manufacturer's instructions. Labeled transferrin was dialyzed thoroughly to remove the unbound dye. $DiIC_{18}(3)$-labeled low density lipoprotein (DiI-LDL) was a gift from Dr. R.N. Ghosh (Cornell University Medical College, NY).

All tissue culture supplies were from GIBCO BRL. All other chemicals were from Sigma Chemical Co.

Cells and Cell Culture

CHO cell lines expressing the human Tf receptor (TRVb-1; McGraw et al., 1987) were grown in bicarbonate-buffered Ham's F-12 medium supplemented with 5% FBS, 100 U/ml penicillin, 100 μg/ml streptomycin, and 200 μg/ml geneticin. Geneticin was used as a selection for the transfected Tf receptors. All cells were grown in a 5% CO_2 environment in humidified incubators set at 37°C. The cells for microscopy were grown on 35-mm plastic tissue culture dishes whose bottoms were replaced with poly-D-lysine–coated coverslips, as described previously (Salzman and Maxfield, 1989). All experimental manipulations as well as microscopy were carried out in these dishes.

Labeling Cells with the Lipid Analogues

Stock solutions of the DiI derivatives were made in ethanol and stored at −86°C under argon. For making the labeling solutions, 750 nmol of $DiIC_{16}(3)$ or 75 nmol of $DiIC_{12}(3)$ or *FAST* DiI were dissolved in 400 μl ethanol. The ethanolic solutions were then injected, while vortexing, into an equimolar amount of fatty acid–depleted BSA in 1 ml PBS at pH 7.4 (final ethanol concentration 40% vol/vol). This mixture was then dialyzed thoroughly against several changes of PBS. As the ethanol was slowly exchanged during dialysis, some of the DiI got transferred to the hydrophobic fatty acid binding sites on the BSA, while much of it self-aggregated, and remained suspended in the labeling solution. The dialysate was then centrifuged twice at 100,000 *g* for 20 min each. When the supernatant from this procedure was run on a Sephacryl S-300 gel filtration column, the DiI eluted as a single peak associated with the BSA. Absorption spectrophotometric analysis showed a loading efficiency (DiI/BSA; mol/mol) of ~0.1 for $DiIC_{16}(3)$, 0.3 for $DiIC_{12}(3)$, and 0.25 for *FAST* DiI. The DiI-loaded BSA solutions were sterilized by passage through 0.2-μm syringe filters and stored at 4°C under argon.

Cells on coverslip-bottom dishes were taken out of the CO_2 incubator, rinsed several times with isotonic Medium 1 (150 mM NaCl, 5 mM KCl, 1 mM $CaCl_2$, 1 mM $MgCl_2$, and 20 mM Hepes, pH 7.4; supplemented with 2 g/liter glucose), and then labeled with an appropriate dilution of a DiI labeling solution (2 μM $DiIC_{16}(3)$, 31 nM $DiIC_{12}(3)$, and 75 nM *FAST* DiI). The concentrations of different DiI derivatives were optimized such that the final concentration of all analogues in the cells (as assessed by integrated fluorescence power per cell) were roughly matched. We used the minimum concentration in each case that would give us a useful fluorescence signal. All labeling reagents were ultracentrifuged at 100,000 *g* for 20 min just before an experiment and equilibrated to 37°C. When cells were labeled using these labeling solutions at 0°C, we obtained very good labeling of the plasma membrane. However, there was also extensive labeling of the background (predominantly the extracellular matrix). This background was dramatically reduced when labeling was instead carried out for a very short time (2 min) at 37°C. Thus, the latter approach was used for all the experiments presented here. After labeling, the cells were rinsed with ice-cold Medium 1 and fixed lightly with 2% paraformaldehyde for 10 min at 0°C.

Fatty-acid free BSA was loaded with the other lipid analogues used in this study using identical procedures. Final concentrations of the different fluorophores used to label cells were 2 μM $DiOC_{16}(3)$, 150 nM *FAST* DiO, 30 nM BODIPY FL C_5-HPC, and 1 μM BODIPY FL C_{12}-HPC.

Endocytosis Assays

Endocytic fates of the DiI derivatives were determined by comparing their intracellular distributions with those of the endocytosed Tf at various time points after the initial loading of the DiI derivatives on to the plasma membranes of TRVb-1 cells. Transferrin, bound to its receptor, was used as a marker for the endocytic recycling route (Dunn et al., 1989; Mukherjee et al., 1997). A comparison of the trafficking of various DiI derivatives with Tf thus allowed us to determine the degree of overlap of the endocytic trafficking routes of these DiI derivatives with that of Tf.

The general experimental methods used to analyze the endocytic behavior of various DiI derivatives were as follows. Cells equilibrated to 37°C were labeled for 2 min at 37°C with the appropriate dilution of a DiI labeling solution, rinsed several times with Medium 1, and then incubated with pre-warmed Oregon green–labeled Tf (OG-Tf; or Alexa 488–conjugated Tf in the confocal experiments) for either 5 or 30 min. At the end of the incubation period, the cells were rinsed with ice-cold Medium 1 and fixed. To confirm the identity of the punctate structures labeled by some DiI derivatives as late endosomes/lysosomes, TRVb-1 cells were labeled with different DiI derivatives as described above, rinsed, and further incubated at 37°C with 1 mg/ml fluorescein-labeled dextrans for 60 min. After the incubation, the cells were rinsed and fixed as described above.

Wide-Field Fluorescence Microscopy and Image Analysis

Fluorescence microscopy and digital image acquisition were carried out using a Leica DMIRB microscope (Leica Mikroscopie und Systeme GmbH) equipped with a cooled CCD camera (Frame Transfer Pentamax camera with a 512 × 512 back-thinned EEV chip, No. 512EFTB; Princeton Instruments) driven by Image-1/MetaMorph Imaging System software (Universal Imaging Corp.). All images were acquired using a high magnification (63×, 1.4 NA) oil immersion objective. DiI derivatives were imaged using a standard rhodamine filter set, while Oregon green was imaged using a fluorescein filter set. The fields to be imaged were chosen on the basis of well spread out cell morphology and the focal plane was chosen to have the structure of interest (e.g., the endocytic recycling compartment [ERC]) in focus in the green (OG-Tf) channel. Choosing the areas for imaging in the non-DiI channel was especially important for the quantitative analyses, since the labeling pattern of the DiI derivatives varied significantly from cell to cell, and this distribution could be potentially skewed by observer bias if the focal plane was chosen in the DiI-labeled fields. We chose Oregon green over fluorescein to label Tf for quantitative microscopy since Oregon green has spectroscopic properties similar to fluorescein, but it has significantly higher photostability and a lower pKa and higher fluorescence yield than fluorescein (Haugland, 1996).

All image analysis was carried out using the Image-1/MetaMorph Imaging System software. For quantitative analyses, the images of cells double labeled with OG-Tf (green) and one of the DiI derivatives (red) and a corresponding differential interference contrast image were sequentially acquired using the CCD camera (12 bit format) and were processed as follows. The fluorescence images were first background corrected by applying a median filter using a 64 × 64 pixel area (0.24 μm/pixel), and the background image was subtracted from the acquired image. The degree of crossover of signal from one channel to the other was determined using cells labeled singly with each of the fluorophores. These images of singly labeled cells were background corrected, followed by measurement of integrated fluorescence intensity in the whole field in both channels. Since autofluorescence was negligible at the exposures used for these experiments, the fluorescence intensity observed in the unlabeled channel (after background subtraction) was taken to represent signal crossover. Crossover measurements were made for four different fields for each fluorophore and averaged to obtain a representative crossover fraction. This crossover fraction of each image was then subtracted from the corresponding image in a double-labeled set before further analysis. The crossover intensity was <2% of the true fluorescence intensity in all cases.

The cell outlines for each set of double-labeled fields were traced out manually in the corresponding differential interference contrast image, and then copied on to the Tf- and DiI-labeled fields. In each cell, the whole cell green (Tf) and red (DiI) fluorescence intensities were measured. Simultaneously in each cell, the relative intensity in the ERC was measured by placing a small box (4 × 4 pixel area) in several locations within the morphologically defined perinuclear recycling compartment. In case of the DiI-labeled fields, precaution was taken not to include any punctate structures that may lie within the rather large area occupied by the ERC. The ratio of fluorescence intensities sampled within the ERCs for the DiI derivative to Tf was then normalized by the whole cell fluorescence intensity ratio for that cell to correct for cell to cell variation in Tf receptor expression and DiI uptake. For the results presented in Figs. 7–9, the measurements were made for ~50 cells in each data set, and the data were collected from experiments carried out on two different days. The validity as well as the limits of this method were first tested using control experiments (see Results).

Confocal Microscopy

Confocal microscopy was performed using an Axiovert 100M inverted microscope equipped with an LSM 510 laser scanning unit and a 63× 1.4 NA plan Apochromat objective (all from Carl Zeiss, Inc.). Samples were excited with a 25-mW argon laser emitting at 458 and 488 nm and a 0.5 mW helium/argon laser emitting at 543 nm; emissions were collected using a 505–530-nm band pass filter to collect green (Alexa 488) emission and a 585-nm long-pass filter to collect red (DiI) emission. Confocal slices were obtained in 0.2-μm increments. The images were collected in eight-bit format, exported from the LSM 510 software, and each confocal slice was

background corrected (using a 64 × 64 pixel median filter) using the MetaMorph software. Summation projection of all background corrected confocal slices were also produced using the MetaMorph software.

For visual output purposes, the digital images (both wide-field and confocal) were clipped to the relevant eight bits, transferred to a Macintosh Power PC, and intensity mapped through logarithmic look up tables (luts) using Adobe Photoshop software and printed on a dye sublimation printer (SpectraStar Dsx; General Parametrics Corp.). For quantitative analyses, the data obtained from MetaMorph Imaging System were routinely transferred to Microsoft Excel spreadsheet software for further calculations.

Results

All DiI Derivatives Show Uniform Labeling of the Plasma Membrane

For our studies, we needed to develop a method of incorporation of different DiI derivatives in the plasma membranes of TRVb-1 cells that would not produce particulates containing DiI. Such particulates could potentially produce artifacts in our experiments, since they could either be pinocytosed by cells or stick nonspecifically to the cell surface and slowly diffuse from there. We found that many previously published labeling protocols produced high levels of aggregated DiI in the aqueous loading buffers. It was difficult to remove these particles by centrifugation since most of these protocols required the use of organic solvents, and at the high speeds necessary to remove all the particles there was a separation of the organic phase with most of the DiI probes dissolved in it. As described in Materials and Methods, we developed a labeling protocol in which DiI derivatives were transferred from an ethanolic stock solution to fatty acid–free BSA in aqueous solution. Ethanol was then removed by dialysis, and the particulates were removed by ultracentrifugation. This method produced a labeling solution with no DiI particles detectable by fluorescence microscopy or gel filtration chromatography. Fig. 2 shows TRVb-1 cells labeled using these DiI/BSA labeling solutions after appropriate dilution at 37°C for 2 min. All three DiI derivatives exhibited plasma membrane labeling with no gross heterogeneity in distribution. There is some variation in intensity that is consistent with surface projections or a small amount of endocytosis during the 2-min incubation. To ensure that the DiI labeling the cell surface had been released from albumin, we did a control experiment in which cells were incubated with a labeling solution containing BSA covalently conjugated to fluorescein (data not shown). No detectable fluorescein signal was left after the labeled BSA was rinsed away.

All DiI Derivatives Enter the Same Sorting Endosomes as Transferrin

Since the DiI derivatives used in this study label the plasma membrane uniformly, they would be expected, a priori, to enter the cells through all available endocytic routes. While these pathways appear to merge at the level of the peripherally distributed tubulovesicular sorting endosomes in most cell types (Tran et al., 1987; Raub et al., 1990), in some cases, such as ruffling A431 cells, they have been reported to remain segregated from each other (Hewlett et al., 1994). It was thus important to document that all the DiI analogues used in this study predominantly entered sorting endosomes, which were characterized by the presence of fluorescent Tf at early times after the initiation of endocytosis of the fluorescent markers. We achieved this by double-labeling TRVb-1 cells for very short times (1 min) with a mixture of 15 μg/ml OG-Tf and each of the DiI derivatives, followed by immediate fixation and looking for colocalization of OG-Tf and the DiI analogues (Fig. 3). Although only a small fraction of the DiI was internalized in 1 min, most vesicles with detectable DiI contain Tf. In some Tf-labeled vesicles, it is difficult to see the DiI because of the high plasma membrane background. We conclude that both Tf and the DiI derivatives enter the same sorting endosomes.

$DiIC_{16}(3)$ Gets Sorted Away from Both FAST DiI and $DiIC_{12}(3)$ after Endocytosis

Intracellular fates of the DiI derivatives were followed by comparing their trafficking to that of receptor-bound OG-Tf, which follows the endocytic recycling pathway. In TRVb-1 cells, Tf exits the sorting endosome with a $t_{1/2}$ of ~2 min and is delivered to the ERC (Dunn et al., 1989; Mayor et al., 1993). Exit from the ERC and delivery to the cell surface occurs with a $t_{1/2}$ of 10–12 min (McGraw et al., 1987; Dunn et al., 1989). In TRVb-1 and other CHO cell lines, the ERC is a collection of narrow tubular elements

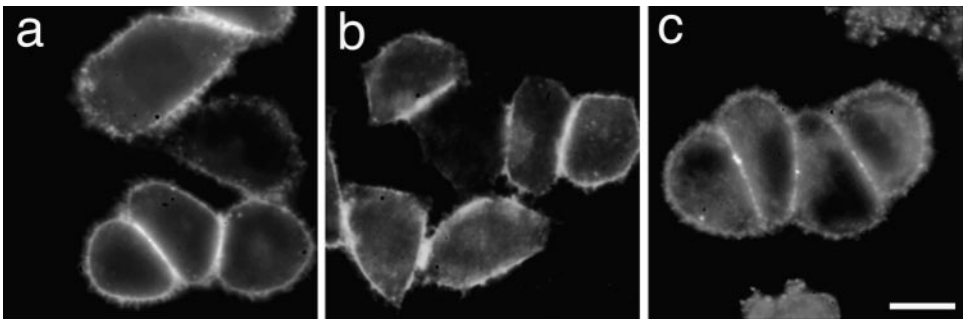

Figure 2. Cell surface (plasma membrane) labeling by (a) $DiIC_{16}(3)$, (b) $DiIC_{12}(3)$, and (c) *FAST* DiI. The cells were labeled for 2 min at 37°C with a final concentration of 2 μM $DiIC_{16}(3)$, 31 nM $DiIC_{12}(3)$, and 75 nM *FAST* DiI. They were then washed several times with ice-cold Medium 1 supplemented with 2 g/liter glucose and fixed with 2% paraformaldehyde for 10 min on ice. The excess paraformaldehyde was rinsed thoroughly and the cells were warmed to room temperature before microscopy. Bar, 10 μm.

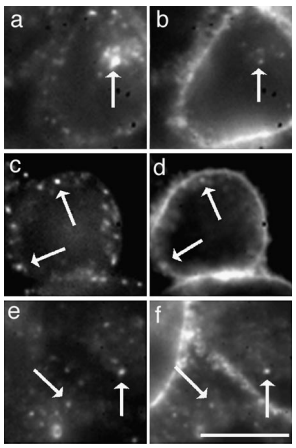

Figure 3. Distribution of receptor-bound Tf and various DiI derivatives in TRVb-1 cells double labeled with OG-Tf and one of the DiI derivatives at very early times after endocytosis. The cells were colabeled for 1 min at 37°C by a mixture containing both the DiI labeling solution (same final concentrations as in Fig. 2) and 15 μg/ml OG-Tf, rinsed once with ice-cold Medium 1, transferred immediately into an ice-water bath to arrest further endocytosis. The cells were then quickly rinsed several times with ice-cold Medium 1 and fixed on ice with prechilled 2% paraformaldehyde for 10 min. Further treatments were identical to those described in Fig. 2. a, c, and e show OG-Tf labeling, while b, d, and f show labeling with $DiIC_{16}(3)$, $DiIC_{12}(3)$, and *FAST* DiI, respectively. Arrows indicate identical positions in matched images to facilitate identification of endosomes that contain both the fluorophores. Bar, 10 μm.

that organize near the microtubule organizing center, and when labeled with a fluorescent marker the ERC appears as a large perinuclear fluorescent spot (Yamashiro et al., 1984). Since exit from the ERC is the slowest step in the endocytic recycling itinerary of the Tf receptor, the ERC is the most brightly labeled structure at steady state (Yamashiro et al., 1984).

The following experiments were designed so that the cell surface Tf receptors would always be saturated with Tf, and the internalization of plasma membrane–associated DiI derivatives could be compared with Tf. Fig. 4 shows cells that were labeled with 2 μM $DiIC_{16}(3)$ for 2 min, washed, and then incubated with 10 μg/ml OG-Tf for 5 (a and b) or 30 (c and d) min. We observe that after 5 min of internalization, OG-Tf is mainly in the ERC, which appears as a single area of fluorescence near the center of each cell (Fig. 4 a). In contrast, a significant fraction of the $DiIC_{16}(3)$ appears in punctate, vesicular structures (Fig. 4 b). A small fraction of $DiIC_{16}(3)$ does appear to codistribute with the Tf at early times. By 30 min, nearly all internalized $DiIC_{16}(3)$ is found to segregate away from Tf, and appears in discrete punctate structures that are distributed throughout the cell (Fig. 4, c and d). In similar experiments (data not shown), we find that even at earlier times after endocytosis (1–5 min) there is never a significant concentration of $DiIC_{16}(3)$ in the pericentriolar area. Most of the $DiIC_{16}(3)$ remains in punctate structures that remain discrete and increase in brightness over this period. This suggests that most $DiIC_{16}(3)$ is retained in the sorting endosome and does not exit along with transferrin receptors that are delivered to the endocytic recycling compartment.

To examine whether the small fraction of $DiIC_{16}(3)$ that appears to colocalize with OG-Tf at 5 min by wide-field microscopy is indeed in the same morphological structures as Tf, we carried out confocal microscopy of cells double labeled with $DiIC_{16}(3)$ and Alexa 488–labeled Tf after a

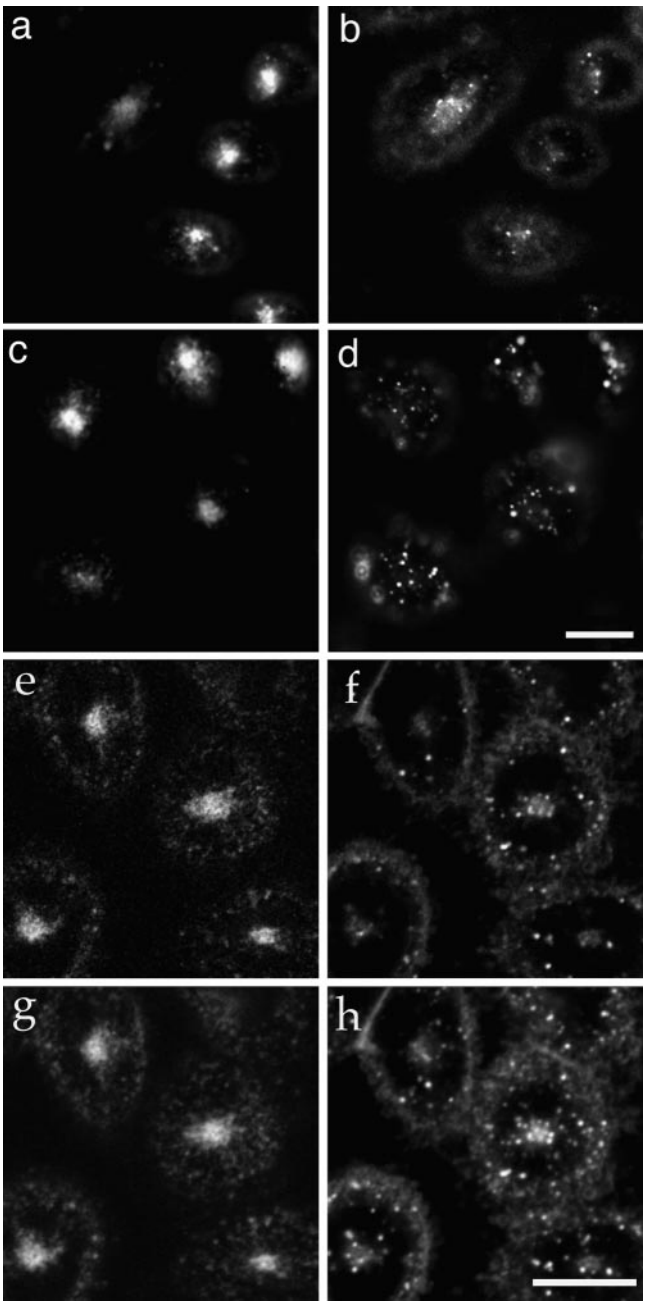

Figure 4. Distribution of receptor-bound OG-Tf (a and c) and $DiIC_{16}(3)$ (b and d) in TRVb-1 cells double labeled with 10 μg/ml OG-Tf and 2 μM $DiIC_{16}(3)$, imaged using wide-field epifluorescence microscopy. The cells were labeled for 2 min at 37°C with $DiIC_{16}(3)$, rinsed, and then incubated further at 37°C in the presence of OG-Tf for 5 (a and b) or 30 (c and d) min. The cells were then washed and fixed as described in Fig. 2. e–h show cells double labeled with 10 μg/ml Alexa 488–Tf and 2 μM $DiIC_{16}(3)$ after 5 min chase, imaged using laser scanning confocal microscopy. e and g show the distributions of Alexa 488–Tf, while f and h show those of $DiIC_{16}(3)$ in the same cells. e and f present a single optical section through the cells, where the ERC is in sharp focus. g and h show summation projection of all the optical slices from the same cells. Bars, 10 μm.

5-min chase. Fig. 4, e and f, shows a single optical section through these cells, while Fig. 4, g and h, shows a summation projection through all the optical sections through the cell. As is clear from Fig. 4, e and f, a fraction of $DiIC_{16}(3)$ at this time does localize to structures that overlap with Tf-containing ERC and cannot be accounted for by out-of-focus fluorescence from late endosomes/lysosomes containing $DiIC_{16}(3)$. However, the summation projection images (Fig. 4, g and h) show that this population represents a small fraction of total intracellular $DiIC_{16}(3)$ fluorescence.

Fig. 5 shows the results from a similar experiment in which the cells were double labeled with OG-Tf (a and c) and $DiIC_{12}(3)$ (b and d), and Fig. 6 shows cells that were double labeled with OG-Tf (a and c) and *FAST* DiI (b and d). Figs. 5 and 6 show the relative distributions of OG-Tf and the DiI derivative after 5 (a and b) and 30 (c and d) min of endocytosis. The DiI derivatives (Figs. 5 and 6, b and d) seem to traffic in a fashion qualitatively similar to Tf (a and c), at least until 30 min after initiation of endocytosis. This was in contrast to the trafficking of $DiIC_{16}(3)$, where after 30 min of endocytosis nearly all $DiIC_{16}(3)$ was found in punctate structures devoid of Tf.

To better understand the trafficking of the DiI derivatives in relatively large cell populations, we carried out a quantitative analysis of the colocalization of various DiI derivatives and Tf in the ERC. The objective was to obtain an estimate of how similar the trafficking of each of the DiI derivatives was to that of Tf, without explicitly defining the alternate destinations of the DiI derivatives. Such an estimate could be obtained from the ratio of the fluorescence intensities of a DiI derivative to that of Tf in the region of the ERC after varying periods of endocytosis. In this analysis, a ratio closer to 1 indicates a trafficking behavior more similar to Tf. To account for differences among cells in the total amount of each fluorophore per cell, we normalized the ratio of fluorescence intensities in the ERC region of every cell to the ratio of the total fluorescence of the two fluorophores in that cell. The details of the image analysis protocol are discussed in Materials and Methods.

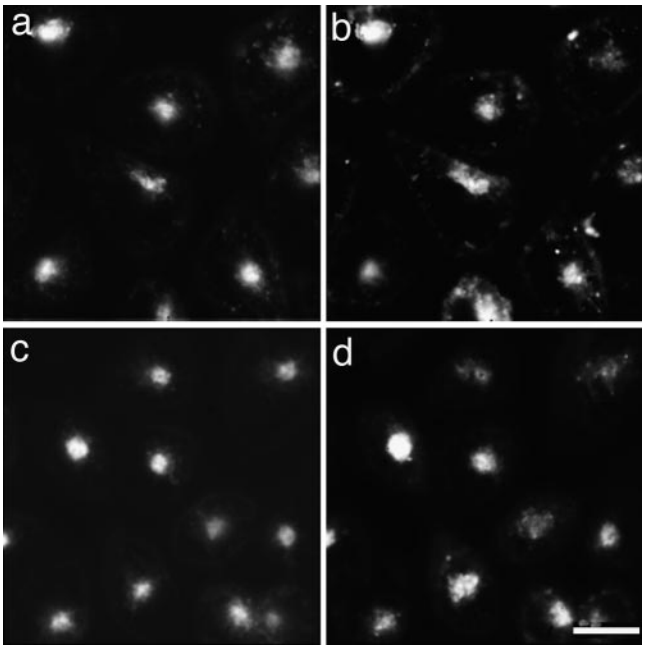

Figure 5. Distribution of receptor-bound OG-Tf (a and c) and $DiIC_{12}(3)$ (b and d) in TRVb-1 cells double labeled with 10 μg/ml OG-Tf and 31 nM $DiIC_{12}(3)$. The cells were labeled for 2 min at 37°C $DiIC_{12}(3)$, rinsed, and then incubated further at 37°C in the presence of OG-Tf for 5 min (a and b) or 30 min (c and d). The cells were then washed and fixed as described in Fig. 2. Bar, 10 μm.

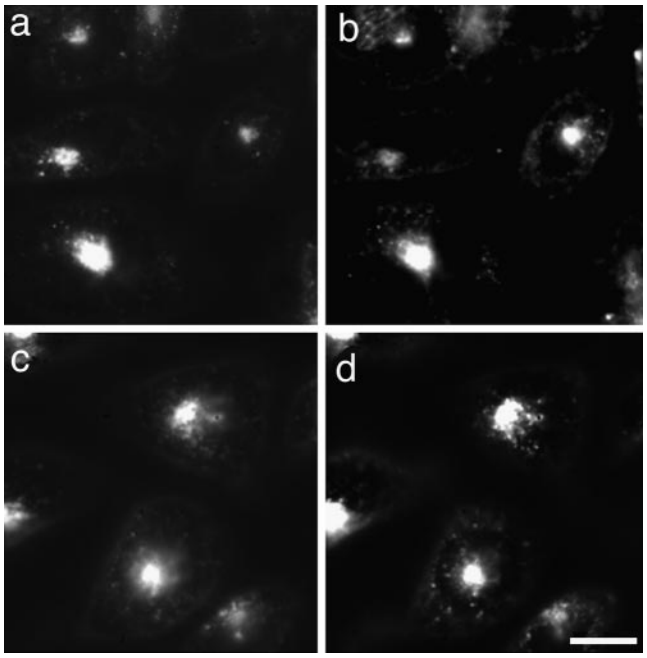

Figure 6. Distribution of receptor-bound OG-Tf (a and c) and *FAST* DiI (b and d) in TRVb-1 cells double labeled with 10 μg/ml OG-Tf and 75 nM *FAST* DiI. The cells were labeled for 2 min at 37°C *FAST* DiI, rinsed, and then incubated further at 37°C in the presence of OG-Tf for 5 (a and b) or 30 (c and d) min. The cells were then washed and fixed as described in Fig. 2. Bar, 10 μm.

We tested the validity of this image analysis protocol and determined the upper and lower limits on the ratios in the ERC that could be reliably measured. In the first test case, the cells were labeled with a mixture of OG-Tf (green fluorescence) and Cy3-Tf (red fluorescence) continuously for 30 min. Fig. 7 a shows a frequency histogram ($n = 50$) comparing the distribution of the two Tfs. As expected for molecules that traffic identically, we obtained a narrow distribution of ratios in the ERC that is centered around 1. To test the case where two probes should sort efficiently from each other, we double-labeled cells with a mixture of DiI-LDL (which is trafficked to the late endosomes) and OG-Tf (which recycles efficiently). The cells were labeled for 5 min with a mixture of both probes at 37°C, followed by a 5-min chase. In this case (Fig. 7 b), we obtained a relatively narrow distribution of ratios of LDL/Tf in the ERC region that was centered around 0.25. The nonzero value of this ratio is due to overlap of the fluorescence from DiI-LDL containing late endosomes/lysosomes that happen to localize in the region of the ERC labeled with OG-Tf. Thus, a test molecule that is completely sorted away from the recycling route would still be ex-

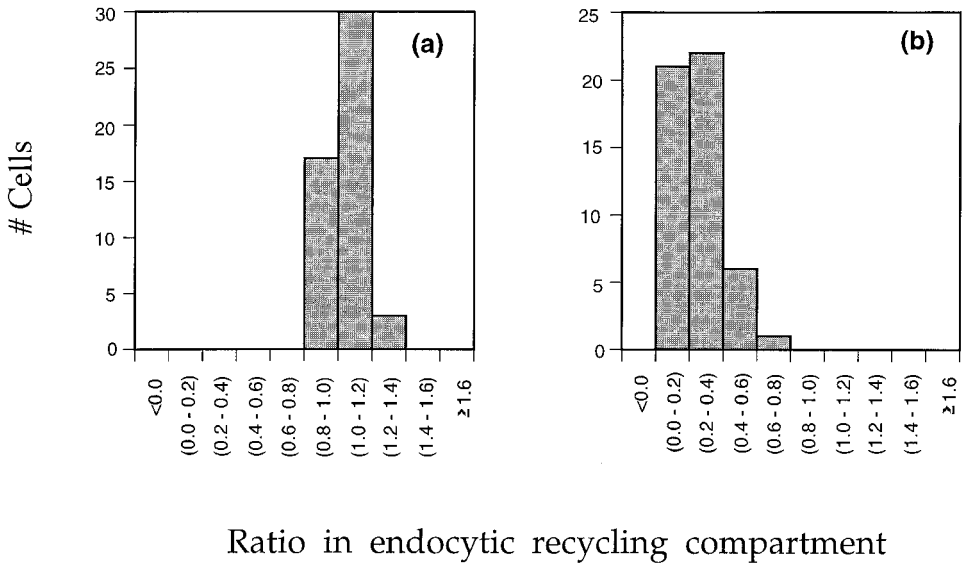

Figure 7. Control experiments to assign limits on the ratios in the ERC that can be reliably measured by our image analysis protocol. (a) A case where both probes traffic identically. TRVb-1 cells were coincubated with 10 μg/ml OG-Tf and 5 μg/ml Cy3-Tf for 30 min at 37°C, and washed and fixed as discussed in Fig. 2. The analysis regime is discussed in detail in Materials and Methods. This figure shows a frequency histogram (n = 50) where the number of cells having ratios of Cy3-Tf/OG-Tf in different ratio intervals are shown. (b) A case where the two probes completely segregate from each other. In this case, cells were coincubated with 1 μg/ml DiI-LDL and 10 μg/ml OG-Tf for 5 min at 37°C, rinsed, chased for another 5 min at 37°C, and fixed as described in Fig. 2. The figure shows a frequency histogram of DiI-LDL/OG-Tf (n = 50).

pected to show a nonzero ratio to Tf in the ERC region using this image analysis protocol.

Fig. 8 shows a quantitative analysis of the ratios of various DiI derivatives to Tf in the ERC regions of TRVb-1 cells (n = 50 for each data set). Fig. 8, a and d, shows the distribution of the ratios in the ERC for $DiIC_{16}(3)$, b and e for $DiIC_{12}(3)$, and c and f for *FAST* DiI. Fig. 9 shows the mean ratio of each DiI derivative to Tf in the ERC at each time point for easier comparison. The analysis shows that even at early times (5 min of endocytosis), the distributions for the three DiI derivatives are significantly different from each other. While *FAST* DiI shows the highest degree of colocalization with Tf in the ERC (ratio centered around 0.8), $DiIC_{16}(3)$ shows the lowest ratio (centered around 0.4) with $DiIC_{12}(3)$ showing an intermediate behavior. This means that *FAST* DiI and $DiIC_{12}(3)$ traffic in a manner more like Tf, compared with $DiIC_{16}(3)$. These results show that sorting of $DiIC_{16}(3)$ occurs relatively quickly after endocytosis, with a significant difference in the ratio in the ERC by 5 min. By 30 min, the differences among various DiI derivatives becomes more pronounced. They all sort away from the Tf recycling pathway to different degrees, with the difference being most pronounced for $DiIC_{16}(3)$ (Fig. 8, a and d). In fact, the distribution of the ratio values for $DiIC_{16}(3)$ to Tf is similar to the distribution for LDL to Tf (Fig. 7 b).

From the results presented above, we find that $DiIC_{16}(3)$ separates from Tf very efficiently following endocytosis into sorting endosomes, and by 30 min its overlap with Tf in the ERC region is similar to the overlap seen for LDL. $DiIC_{12}(3)$ and *FAST* DiI show greater overlap with Tf. However, in none of these cases does the ratio of a DiI derivative to Tf reach 1 (as seen when two differently tagged Tfs are used to label the cells). This indicates that the DiI derivatives exhibit a range of partitioning preferences that lead to differential trafficking, and the sorting is not all-or-none. We also note that the distributions of the ratios of various DiI derivatives to Tf in the ERCs of CHO cells (Fig. 8) are significantly wider than a similar distribution for the cells double labeled with Cy3-Tf/OG-Tf or LDL/Tf (Fig. 7). This is indicative of cell-to-cell variability in the trafficking of the DiI derivatives. The basis for this heterogeneity is unknown.

$DiIC_{16}(3)$ Preferentially Enters Late Endosomes/Lysosomes

We used colocalization with high molecular weight fluorescein-labeled dextrans as an assay to test whether the punctate structures that contained the DiI derivatives at later times were late endosomes/lysosomes. In Fig. 10, we show a colocalization of the various DiI derivatives with fluorescein dextran after a 60-min chase. The cells were labeled for 2 min at 37°C with each DiI derivative, washed, and then incubated for 60 min in the presence of 1 mg/ml fluorescein dextran. Fig. 10, a, c, and e, shows the distribution of fluorescein dextran in cells double labeled with $DiIC_{16}(3)$ (b), $DiIC_{12}(3)$ (d), and *FAST* DiI (f). Fig. 10, a and b, shows a substantial overlap between $DiIC_{16}(3)$ and fluorescein dextran after a 1-h chase, with a more modest fraction of either $DiIC_{12}(3)$ (c and d) or *FAST* DiI (e and f) entering these compartments. Fluorescence from the DiI derivatives in the ERC is not seen in Fig. 10 because the ERC is at a higher focal plane than the late endosomes in most cells. These results show that, among the DiI derivatives investigated in this paper, only $DiIC_{16}(3)$ enters late endosomes/lysosomes in significant proportions.

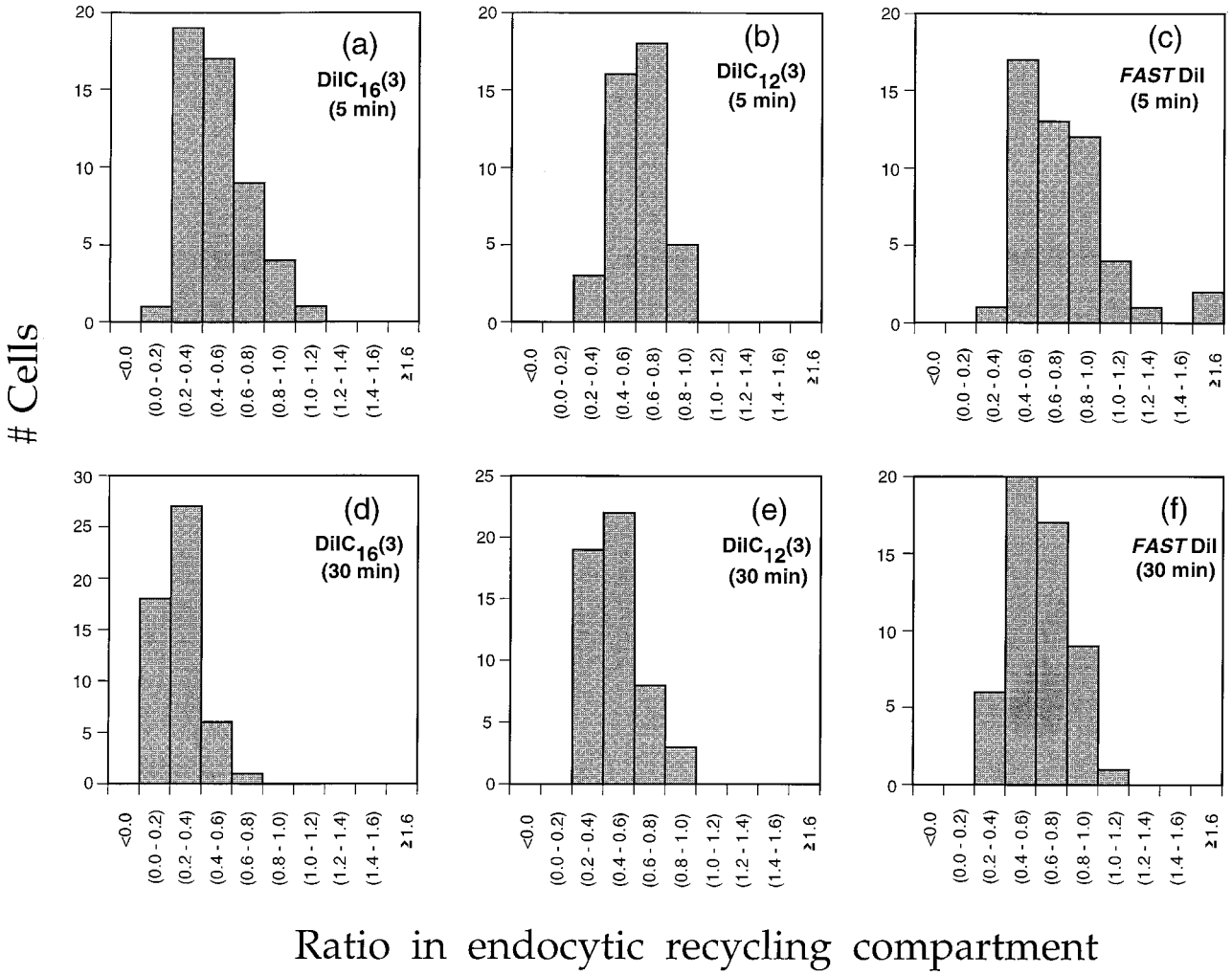

Figure 8. Quantitative analysis of the results presented in Figs. 4–6. The results are shown as frequency histograms of the ratio of the various DiI derivatives to Tf in the ERC at various time points. a–c show the ratios in the ERC after 5 min, while d–f show them after 30 min. $DiIC_{16}(3)$ (a and d), $DiIC_{12}(3)$ (b and e), and *FAST* DiI (c and f).

Endocytic Sorting of Lipid Analogues Based on the Chemistry of Their Tails Is Not Unique to the DiI Derivatives

To ensure that the endocytic sorting of the DiI derivatives reported in this paper is not unique to these fluorophores, we conducted similar experiments with two other sets of lipid analogues. One set, $DiOC_{16}(3)$ and *FAST* DiO, were identical to the DiI analogues except that they contained an oxygen atom instead of a carbon atom attached to two methyl groups in their head groups (see Fig. 1). Both DiO derivatives contained long chains, but in the former case they were both saturated, while in the latter they contained two double bonds each. The other set constituted of two analogues of phosphatidylcholine, which both had one saturated 16-carbon tail, whereas the second tail contained a BODIPY FL fluorophore at the end of either a 5- or a 12-carbon acyl chain (BODIPY FL C_5-HPC and BODIPY FL C_{12}-HPC, respectively; see Fig. 1).

Fig. 11 shows the distribution of these lipid analogues in TRVb-1 cells singly labeled with each fluorophore. Cells were labeled with 150 nM *FAST* DiO (Fig. 11 a), 2 μM $DiOC_{16}(3)$ (Fig. 11 b), 30 nM BODIPY FL C_5-HPC (Fig. 11 c), and 1 μM BODIPY FL C_{12}-HPC (Fig. 11 d). For each type of lipid analogue, the concentrations of the labeling solutions were adjusted to provide approximately the same level of incorporation in the cells. The cells were labeled for 2 min at 37°C with each labeling solution, rinsed, incubated further at 37°C in Medium 1 for 30 min, and then fixed lightly with paraformaldehyde. The results show that while the lipid analogues with unsaturations in their tails (e.g., *FAST* DiO; Fig. 11 a) or containing one short tail (e.g., BODIPY FL C_5-HPC; Fig. 11 c) predominantly entered a central fluorescent compartment; lipid analogues containing long saturated tails (e.g., $DiOC_{16}(3)$; Fig. 11 b and BODIPY FL C_{12}-HPC; Fig. 11 d) entered punctate structures distributed throughout the cells. Double-labeling studies (data not shown) confirm the identities of the central fluorescent compartment as the ERC and the punctate structures as late endosomes/lysosomes. We do observe some differences in the degrees to which

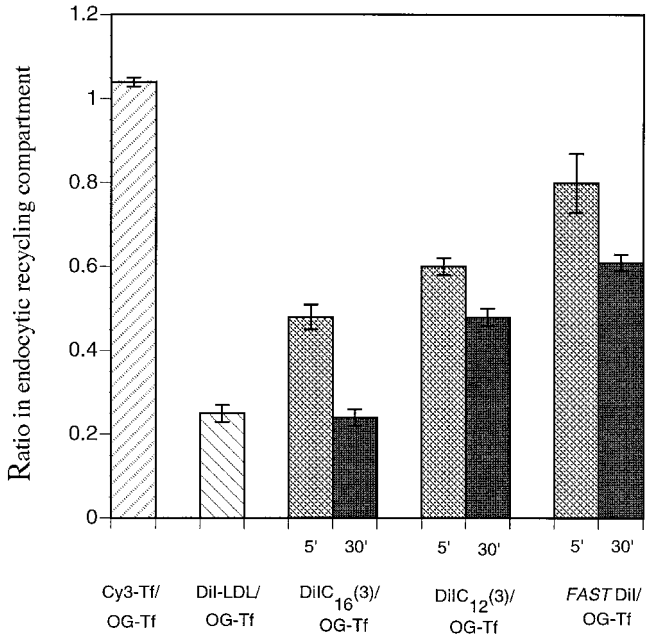

Figure 9. The mean values for the ratios of various DiI derivatives to OG-Tf in the ERC after 5 or 30 min of endocytosis. The values were obtained from the frequency distributions presented in Figs. 7 and 8. Bars represent the standard errors in the data.

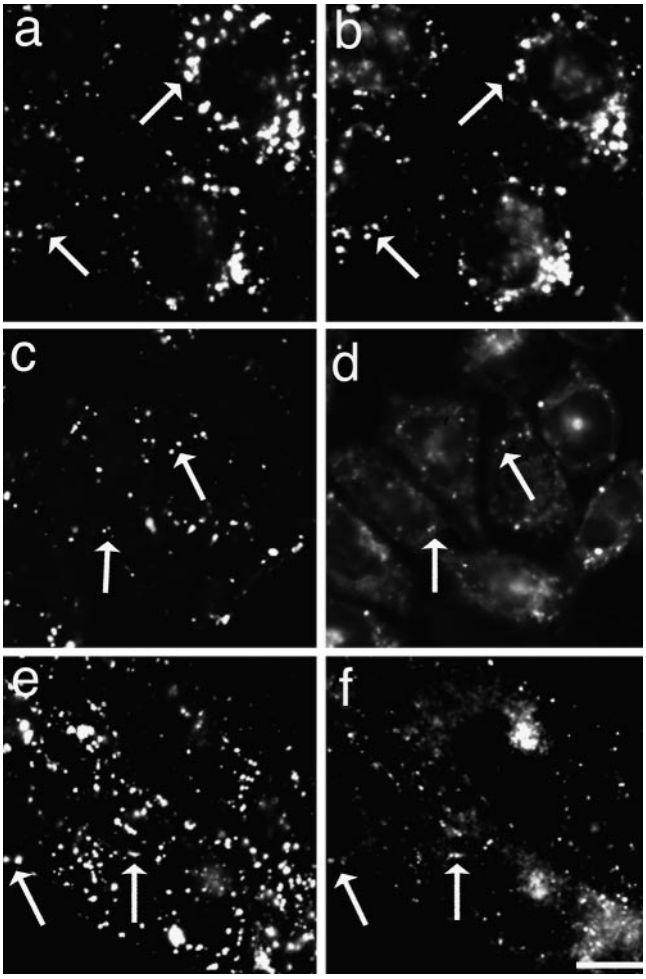

Figure 10. Distribution of fluorescein-dextran and the various DiI derivatives in TRVb-1 cells double labeled with 1 mg/ml fluorescein-dextran (a, c, and e) and 2 mM $DiIC_{16}(3)$ (b), 21 nM $DiIC_{12}(3)$ (d), and 75 nM *FAST* DiI (f), respectively. The cells were labeled for 2 min at 37°C with the DiI labeling solution, rinsed, and then incubated further at 37°C in the presence of fluorescein-dextran for 60 min. Further treatments were identical to those described in Fig. 2. Arrows indicate endosomes that contain both the fluorophores. Bar, 10 μm.

$DiOC_{16}(3)$ and BODIPY FL C_{12}-HPC are directed to the late endocytic pathway. While $DiOC_{16}(3)$ appears to be as efficient as $DiIC_{16}(3)$ in being delivered to the late endosomes in 30 min, we see a larger fraction of BODIPY FL C_{12}-HPC in the ERC at this time. However, as seen in Fig. 11, the difference between these analogues and the corresponding analogues with unsaturated and short chains is very clear. These results are similar to our observations with the DiI analogues in which lipid analogues with short or unsaturated tails recycle efficiently, but those with long and saturated tails are preferentially directed to the late endocytic pathway.

Discussion

The results presented here show that different DiI derivatives, varying solely in the composition of their alkyl chains, exhibit differential trafficking after their internalization from the cell surface into sorting endosomes. While the DiI derivative with long and saturated tails [i.e., $DiIC_{16}(3)$] preferentially enters the late endocytic pathway, the derivatives with shorter [$DiIC_{12}(3)$] or unsaturated (*FAST* DiI) tails are efficiently delivered to the ERC. These observations are reinforced by two other sets of lipid analogues.

There are several steps along the endocytic pathway where sorting of different DiI analogues could have occurred. First, some of the segregation might have occurred at the plasma membrane. Domains enriched in $DiIC_{16}(3)$ have been observed on the plasma membrane of rat basophil leukemia cells when IgE receptors are cross-linked (Thomas et al., 1994). Although we did not detect any inhomogeneity in the distribution of the DiI derivatives on the cell surface, we cannot rule out submicroscopic segregation and/or variations in the rates of internalization of different DiI derivatives. However, even if cell surface heterogeneity is present, it could not account for the sorting we observe between $DiIC_{16}(3)$ and the other two DiI derivatives, since we report that all DiI derivatives initially enter sorting endosomes that also contain endocytosed Tf. Thus, most of the sorting must take place at a step after the internalization of $DiIC_{16}(3)$ and Tf into common sorting endosomes.

The sorting endosomes serve as the branch point for entry into either the recycling route or the late endocytic route. We propose that this is the major site where $DiIC_{16}(3)$ sorts out of the endocytic recycling route. This site of sorting is consistent with the fact that the sorting occurs as early as 5 min after endocytosis. $DiIC_{16}(3)$ is retained in punctate endosomes while *FAST* DiI begins to

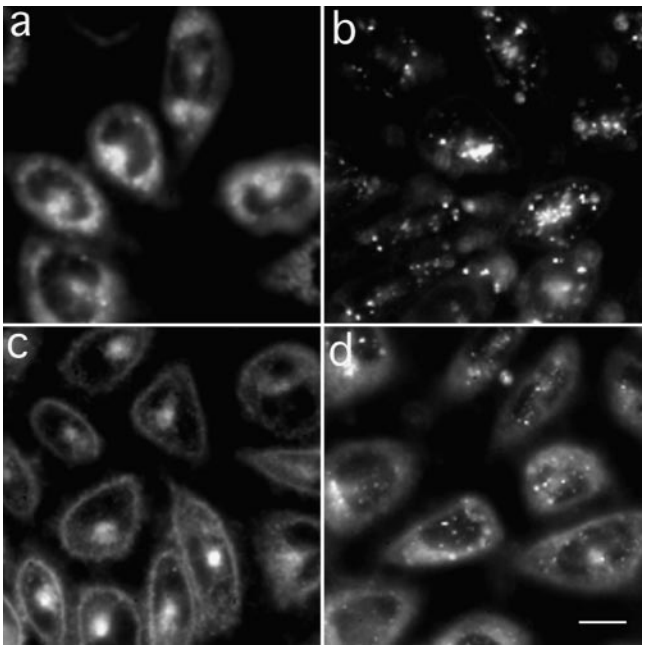

Figure 11. Distribution of lipid analogues in TRVb-1 cells. Cells were labeled with 150 nM *FAST* DiO (a), 2 μM $DiOC_{16}(3)$ (b), 30 nM BODIPY FL C_5-HPC (c), or 1 μM BODIPY FL C_{12}-HPC (d). The cells were labeled for 2 min at 37°C with each labeling solution, rinsed, and then incubated further at 37°C in Medium 1 for 30 min. Further treatments were identical to those described in Fig. 2. Bar, 10 μm.

enter the ERC within 5 min. As expected for a molecule that is retained in the sorting endosomes, nonrecycled $DiIC_{16}(3)$ is subsequently delivered to the late endosomes (Fig. 10).

The retention of $DiIC_{16}(3)$ in the sorting endosomes and its subsequent delivery to the late endocytic structures does not appear to be determined, in any significant way, by specific lipid–protein interaction with some transmembrane protein. In control experiments (data not shown), we have seen that $DiIC_{16}(3)$ is delivered to late endosomes even when the cells are labeled with 10-fold more $DiIC_{16}(3)$ than used in the experiments reported in this study. It has been estimated in the case of rat basophilic leukemia cells that optimal labeling of the cell surface with $DiIC_{16}(3)$ results in $\sim 10^7$–10^8 DiI molecules per cell (Thomas et al., 1994). On the contrary, even a highly expressed protein on the cell surface has $\sim 10^5$–10^6 copies (Ryan et al., 1988; Gennis, 1989). Considering that such a protein would also interact with native lipids, it seems unlikely that stoichiometric binding to any transmembrane protein or even a group of proteins would redirect all $DiIC_{16}(3)$ to the late endosomes. In contrast, if lateral membrane domains of varying fluidity and/or curvatures did exist in the membranes of the sorting endosomes, $DiIC_{16}(3)$, by virtue of its long saturated alkyl chains, would partition preferentially into the more rigid domains or those with a convex curvature. We show several variations of these possibilities in Fig. 12. We suggest that if any specific lipid–protein interaction has to occur, it would be feasible only within the context of fluidity- or curvature-dependent cosegregation of the lipids and proteins in question, so that high enough effective concentrations can be achieved.

Domain-based Segregation in the Sorting Endosomes: A Working Hypothesis

The differential trafficking of the lipid analogues with long saturated hydrophobic tails relative to those with short or unsaturated tails can be rationalized if the vesicular region of the sorting endosomes are considered to represent membrane domains that are more rigid than those in the attached tubules that bud from the sorting endosomes [see Fig. 12, (1)]. There is evidence that narrow tubules in model membrane systems are enriched in more fluid domains. For example, when either gel or fluid phase liposomes were subjected to suction by a micropipette, it was found to be easier to pull fluid membranes into long narrow tubules in response to suction as compared with membranes in the gel phase (Evans and Needham, 1987). Further, a study that measured diffusion coefficients of transmembrane proteins in red blood cell "tethers" (hollow membranous cylinders, up to 36 μm long and ~100 nm in diameter) found a dramatic increase in the diffusion coefficients of these proteins in the tether membrane (Berk and Hochmuth, 1992). In an alternate model, the bilayer fluidity in both the vesicular and the tubular parts of the sorting endosome could be roughly similar, except that the necks joining the tubules to the vesicle, which are under high curvature stress, would be specifically enriched in lipids that can be accommodated in regions of high curvature [Fig. 12, (2)]. In this case, any lipid analogue that cannot easily traverse this small but highly curved fluid (disordered) domain at the neck of the tubule would be preferentially retained in the sorting endosome. Both alternatives are feasible and have been proposed previously in biophysical treatments of bud formation in model membranes (Lipowsky, 1993; Sackmann and Feder, 1995).

In addition, the shape of an amphiphile can be related to its propensity to induce curvature in model membranes, as well as to partition preferentially into preexisting membrane domains of varying curvatures (Cullis and de Kruijff, 1979; Gennis, 1989). More precisely, if a molecule has approximately equal cross-sectional areas in its head group and tail region, the molecule can be considered as a cylinder that does not induce any curvature in a bilayer and would preferentially partition into planar regions of the membrane (no curvature preference). On the other hand, amphiphiles with larger (an inverted cone) or smaller (a cone) head group cross-sectional areas would induce opposite curvatures or partition into preexisting regions of opposite curvature. Since $DiIC_{16}(3)$, with its alkyl tails stretched out all-trans, would approximate an inverted cone, it would be expected to preferentially enter intralumenal invaginations or involutions in the sorting endosome membrane and hence segregate from the recycling pool of membrane-bound molecules [Fig. 12, (3)]. *FAST* DiI, on the other hand, would look more like a cylinder or a cone (depending on the number of gauche conformations in the alkyl tails in addition to the two cis double bonds) and hence would have either no curvature preference or a preference for concave curvatures that would result in its enhanced entry into the tubules of the sorting en-

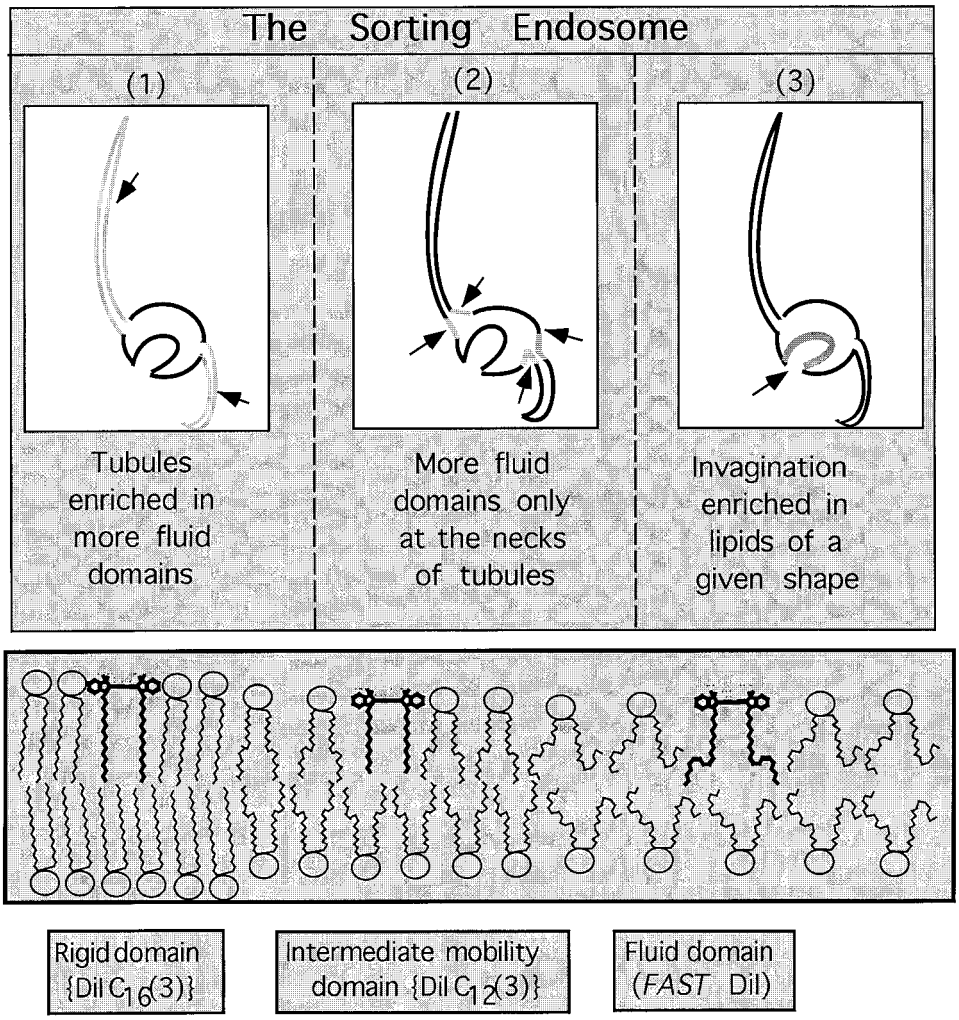

Figure 12. A schematic representation of the endocytic sorting of lipid analogues occurring at the sorting endosomes. Molecules internalized from the cell surface enter the tubulovesicular sorting endosomes. Here, most of the surface area (including most of the membrane-bound molecules) are in the long tubular projections that repeatedly pinch off and deliver their contents to the recycling route, while some membrane components are specifically retained in this organelle and are eventually delivered to late endosomes. Such sorting out of the recycling route would require that these molecules do not enter the tubules that contain material destined to recycle. Here, we propose mechanisms that could act to constrain a fraction of membrane-bound molecules in the membrane surrounding the spherical part of the sorting endosome. (1) The tubules could be enriched in more fluid domains so that lipids that preferentially partition into such domains [e.g., $DiIC_{12}(3)$ and *FAST* DiI] would be enriched there, while rigid domain–preferring lipids such as $DiIC_{16}(3)$ could be depleted. (2) The necks of the tubules could represent extremely fluid domains (due to excessive curvature stress), and only those membrane components that can traverse these domains would be able to enter the tubules in significant proportions. (3) Certain lipids such as $DiIC_{16}(3)$ may be enriched in the invaginations of the vesicular region of the sorting endosome by virtue of their inverted cone shape. See text for more detailed discussion. The above possibilities are not mutually exclusive.

dosomes. This difference in shape might partly explain why $DiIC_{12}(3)$ recycles less efficiently than *FAST* DiI even though both have similar fluidity preferences.

From the sorting endosomes, most membrane-bound components enter the ERC and are recycled out to the cell surface with a half time of 10–12 min. The ERC has been shown to have sorting functions of its own (Johnson et al., 1993, 1998; Presley et al., 1993; Marsh et al., 1995). Recent studies show that glycosylphosphatidylinositol (GPI)–anchored proteins are recycled approximately three times more slowly than C_6-NBD-SM or Tf receptor (Mayor et al., 1998). The recycling of GPI-anchored proteins can be restored to the same rate as Tf receptor when the cells are grown in media that lower cellular cholesterol by ~40% (Mayor et al., 1998). Cholesterol is known to be a major modulator of bilayer motional characteristics and to be involved in the formation of ordered domains in model membrane systems (Yeagle, 1985; Schroeder et al., 1995). The cholesterol dependence suggests the involvement of ordered lipid domains in the slow recycling of GPI-anchored proteins. The ERC does not, however, appear to be a major site for the sorting of $DiIC_{16}(3)$ from other recycling markers, since at no time during its endocytic itinerary do we see a significant concentration of $DiIC_{16}(3)$ in the ERC. As seen in Fig. 4, there is a minor fraction of $DiIC_{16}(3)$ that appears to localize at the ERC by optical microscopy. Even though some $DiIC_{16}(3)$ appears to enter the ERC, its efficiency of sorting to late endosomes would be comparable with that found for ligands that bind to receptors. For example, ~20% of all internalized α_2-macroglobulin (Yamashiro et al., 1989) and ~40% of insulin (Levy and Olefsky, 1987) are recycled undegraded during each endocytic passage through the cell.

Several previously reported examples of lipid sorting can be understood in terms of our working hypothesis based on lipid shapes and fluidity preferences. For example, C_6-NBD-SM and related lipid analogues that recycle efficiently contain one very short (6-carbon) acyl chain to which the reporter group is attached. The polar NBD group would make this tail loop up to the membrane inter-

face (Chattopadhyay and London, 1987), so that the total cross-sectional area occupied by this molecule would be quite large. These factors would be expected to result in preferential partitioning of this lipid analogue to more fluid regions of the bilayer, and thus would be predicted by our model to predominantly enter the endocytic recycling pathway. On the other hand, some lipids that have been reported to be targeted to late endocytic compartments contain long, saturated acyl chains (e.g., rhodamine-labeled phosphatidylethanolamine and some glycosphingolipids; Kok et al., 1990, 1991) that would result in their preferential partitioning to the more rigid parts of the bilayer. In fact, Sandhoff and Klein (1994) have suggested that the retention of certain lipid components such as glycosphingolipids in the inner involutions of the endosomes may play a role in their eventual delivery to the degradative pathway.

Our observations are also consistent with the recent observations of Chen et al. (1997). This study used fibroblasts whose plasma membranes were labeled with a BODIPY FL–labeled lipid analogue that fluoresced green at low concentrations (monomer fluorescence) and red at high concentrations (excimer fluorescence). The plasma membranes for these experiments were labeled such that all the cell surface fluorescence was only monomer (green) fluorescence. Interestingly, when these cells were allowed to endocytose for as short as 7 s, it was found that, while some newly formed endosomes still fluoresced green, others in the same cell exhibited red (excimer) fluorescence. All plasma membrane fluorescence still remained green. These observations could either mean that the lipid analogue segregated into lateral domains more or less enriched in this analogue just before being endocytosed, or that all endosomes contain a roughly similar number of copies of the fluorescent lipid analogue, but that in a subset of those endosomes the analogue segregated into subdomains, thereby increasing their effective concentration and giving rise to excimer fluorescence. Both these possibilities would be consistent with our working hypothesis for lipid sorting in fibroblasts.

Sorting of lipids occurs at many membrane trafficking steps. For example, the sorting of $DiIC_{16}(3)$ out of the recycling pathway occurs primarily at the sorting endosomes, while GPI-anchored proteins are delayed in their export from the ERC. Similarly, the TGN has been reported by several groups to be the primary site along the biosynthetic pathway for sorting of apically and basolaterally destined lipids (Simons and van Meer, 1988). It is conceivable that lipid sorting occurs to some extent at every step where a vesicle or tubule buds from an organelle. We emphasize that the possibilities presented in our model are neither exhaustive nor mutually exclusive. On the contrary, they are presented solely as pointers toward the various possibilities that are conceivable. In general, the principles involved in this type of sorting include the chemistry of the individual membrane component and the composition of the host bilayer. The process we observe in endosomes may very well reflect a more ubiquitous mechanism in several intracellular sorting processes. This would offer an energetically inexpensive mechanism for a relatively efficient sorting of certain classes of molecules from others (Parsegian, 1995). In the cellular milieu, such mechanisms would act in concert with other, more specific, protein–protein or protein–lipid interactions that could modulate or "fine-tune" this basal level sorting.

We thank Drs. Tim McGraw, Bill Mallet, Lynda Pierini, and Richik Ghosh for critical reading of the manuscript and for helpful discussions.

S. Mukherjee acknowledges a postdoctoral fellowship from the Norman and Rosita Winston Foundation for Biomedical Research. The study was supported by grant DK27083 from the National Institutes of Health and by a grant from the Human Frontier Science Program.

Received for publication 3 March 1998 and in revised form 10 February 1999.

References

Axelrod, D. 1979. Carbocyanine dye orientation in red cell membrane studied by microscopic fluorescence polarization. *Biophys. J.* 26:557–574.

Berk, D.A., and R.M. Hochmuth. 1992. Lateral mobility of integral proteins in red blood cell tethers. *Biophys. J.* 61:9–18.

Brown, D.A., and E. London. 1997. Structure of detergent-resistant membrane domains: does phase separation occur in biological membranes? *Biochem. Biophys. Res. Commun.* 240:1–7.

Callaghan, R., L.C.M. van Gorkom, and R.M. Epand. 1992. A comparison of membrane properties and composition between cell lines selected and transfected for multi-drug resistance. *Br. J. Cancer.* 66:781–786.

Chattopadhyay, A., and E. London. 1987. Parallax method for direct measurement of membrane penetration depth utilizing fluorescence quenching by spin-labeled phospholipids. *Biochemistry*. 26:39–45.

Chen, C.S., O.C. Martin, and R.E. Pagano. 1997. Changes in the spectral properties of a plasma membrane lipid analog during the first seconds of endocytosis in living cells. *Biophys. J.* 72:37–50.

Cullis, P.R., and B. de Kruijff. 1979. Lipid polymorphism and the functional roles of lipids in biological membranes. *Biochim. Biophys. Acta.* 559:399–420.

Dunn, K.W., T.E. McGraw, and F.R. Maxfield. 1989. Iterative fractionation of recycling receptors from lysosomally destined ligands in an early sorting endosome. *J. Cell Biol.* 109:3303–3314.

Evans, E., and D. Needham. 1987. Physical properties of surfactant bilayer membranes: thermal transitions, elasticity, rigidity, cohesion, and colloidal interactions. *J. Phys. Chem*. 91:4219–4228.

Friedrichson, T., and T.V. Kurzchalia. 1998. Microdomains of GPI-anchored proteins in living cells revealed by crosslinking. *Nature*. 394:802–805.

Gennis, R.B. 1989. Biomembranes: Molecular Structure and Function. Springer-Verlag, New York.

Haugland, R.P. 1996. Handbook of Fluorescent Probes and Research Chemicals. Molecular Probes, Inc., Eugene, OR.

Hewlett, L.J., A.R. Prescott, and C. Watts. 1994. The coated pit and macropinocytic pathways serve distinct endosome populations. *J. Cell Biol.* 124:689–703.

Johnson, A.O., A. Subtil, R. Petrush, K. Kobylarz, S.R. Keller, and T.E. McGraw. 1998. Identification of an insulin-responsive, slow endocytic recycling mechanism in Chinese hamster ovary cells. *J. Biol. Chem*. 273:17968–17977.

Johnson, I.D., H.C. Kang, and R.P. Haugland. 1991. Fluorescent membrane probes incorporating dipyrrometheneboron difluoride fluorophores. *Anal. Biochem*. 198:228–237.

Johnson, K.F., and S. Kornfeld. 1992. A His-Leu-Leu sequence near the carboxyl terminus of the cytoplasmic domain of the cation-dependent mannose 6-phosphate receptor is necessary for the lysosomal enzyme sorting function. *J. Biol. Chem*. 267:17110–17115.

Johnson, L.S., K.W. Dunn, B. Pytowski, and T.E. McGraw. 1993. Endosome acidification and receptor trafficking: bafilomycin A1 slows receptor externalization by a mechanism involving the receptor's internalization motif. *Mol. Biol. Cell*. 4:1251–1266.

Klausner, R.D., and D.E. Wolf. 1980. Selectivity of fluorescent lipid analogues for lipid domains. *Biochemistry*. 19:6199–6203.

Kobayashi, T., E. Stang, K.S. Fang, P. de Moerloose, R.G. Parton, and J. Gruenberg. 1998. A lipid associated with antiphospholipid syndrome regulates endosome structure and function. *Nature*. 392:193–197.

Kok, J.W., T. Babia, and D. Hoekstra. 1991. Sorting of sphingolipids in the endocytic pathway of HT29 cells. *J. Cell Biol.* 114:231–239.

Kok, J.W., M. ter Beest, G. Scherphof, and D. Hoekstra. 1990. A non-exchangeable fluorescent phospholipid analog as a membrane traffic marker of the endocytic pathway. *Eur. J. Cell Biol.* 53:173–184.

Koval, M., and R.E. Pagano. 1989. Lipid recycling between the plasma membrane and intracellular compartments: transport and metabolism of fluorescent sphingomyelin analogues in cultured fibroblasts. *J. Cell Biol.* 108:2169–2181.

Levy, J.R., and J.M. Olefsky. 1987. The trafficking and processing of insulin and insulin receptors in cultured hepatocytes. *Endocrinology*. 121:2075–2086.

Lipowsky, R. 1993. Domain-induced budding of fluid membranes. *Biophys. J.* 64:1133–1138.

Mackinnon, W.B., G.L. May, and C.E. Mountford. 1992. Esterified cholesterol

and triglyceride are present in plasma membranes of Chinese hamster ovary cells. *Eur. J. Biochem.* 205:827–839.
Marsh, E.W., P.L. Leopold, N.L. Jones, and F.R. Maxfield. 1995. Oligomerized transferrin receptors are selectively retained by a lumenal sorting signal in a long-lived endocytic recycling compartment. *J. Cell Biol.* 129:1509–1522.
Mayor, S., J.F. Presley, and F.R. Maxfield. 1993. Sorting of membrane components from endosomes and subsequent recycling to the cell surface occurs by a bulk flow process. *J. Cell Biol.* 121:1257–1269.
Mayor, S., S. Sabharanjak, and F.R. Maxfield. 1998. Cholesterol-dependent retention of GPI-anchored proteins in endosomes. *EMBO (Eur. Mol. Biol. Organ.) J.* 17:4626–4638.
McGraw, T.E., L. Greenfield, and F.R. Maxfield. 1987. Functional expression of the human transferrin receptor cDNA in Chinese hamster ovary cells deficient in endogenous transferrin receptor. *J. Cell Biol.* 105:207–214.
Mouritsen, O.G., and K. Jorgensen. 1995. Micro-, nano- and meso-scale heterogeneity of lipid bilayers and its influence on macroscopic membrane properties. *Mol. Membr. Biol.* 12:15–20.
Mukherjee, S., R.N. Ghosh, and F.R. Maxfield. 1997. Endocytosis. *Physiol. Rev.* 77:759–803.
Opresko, L.K., C.P. Chang, B.H. Will, P.M. Burke, G.N. Gill, and H.S. Wiley. 1995. Endocytosis and lysosomal targeting of epidermal growth factor receptors are mediated by distinct sequences independent of the tyrosine kinase domain. *J. Biol. Chem.* 270:4325–4333.
Parsegian, V.A. 1995. The cows or the fence? *Mol. Membr. Biol.* 12:5–7.
Pierini, L., D. Holowka, and B. Baird. 1996. FcεRI-mediated association of 6-μm beads with RBL-2H3 mast cells results in exclusion of signaling proteins from the forming phagosome and abrogation of normal downstream signaling. *J. Cell Biol.* 134:1427–1439.
Presley, J.F., S. Mayor, K.W. Dunn, L.S. Johnson, T.E. McGraw, and F.R. Maxfield. 1993. The End2 mutation in CHO cells slows the exit of transferrin receptors from the recycling compartment but bulk membrane recycling is unaffected. *J. Cell Biol.* 122:1231–1241.
Raub, T.J., M.J. Koroly, and R.M. Roberts. 1990. Endocytosis of wheat germ agglutinin binding sites from the cell surface into a tubular endosomal network. *J. Cell. Physiol.* 143:1–12.
Ryan, T.A., J. Myers, D. Holowka, B. Baird, and W.W. Webb. 1988. Molecular crowding on the cell surface. *Science.* 239:61–64.
Sackmann, E., and T. Feder. 1995. Budding, fission and domain formation in mixed lipid vesicles induced by lateral phase separation and macromolecular condensation. *Mol. Membr. Biol.* 12:21–28.
Salzman, N.H., and F.R. Maxfield. 1989. Fusion accessibility of endocytic compartments along the recycling and lysosomal endocytic pathways in intact cells. *J. Cell Biol.* 109:2097–2104.
Sandhoff, K., and A. Klein. 1994. Intracellular trafficking of glycosphingolipids: role of sphingolipid activator proteins in the topology of endocytosis and lysosomal digestion. *FEBS Lett.* 346:103–107.
Schroeder, F., J.K. Woodford, J. Kavecansky, W.G. Woods, and C. Joiner. 1995. Cholesterol domains in biological membranes. *Mol. Membr. Biol.* 12: 113–119.
Simons, K., and E. Ikonen. 1997. Functional rafts in cell membranes. *Nature.* 387:569–572.
Simons, K., and G. van Meer. 1988. Lipid sorting in epithelial cells. *Biochemistry.* 27:6197–6202.
Sims, P.J., A.S. Waggoner, C.-H. Wang, and J.F. Hoffman. 1974. Studies on the mechanism by which cyanine dyes measure membrane potential in red blood cells and phosphatidylcholine vesicles. *Biochemistry.* 13:3315–3330.
Spink, C.H., M.D. Yeager, and G.W. Feigenson. 1990. Partitioning behavior of indocarbocyanine probes between coexisting gel and fluid phases in model membranes. *Biochim. Biophys. Acta.* 1023:25–33.
Thomas, J.L., D. Holowka, B. Baird, and W.W. Webb. 1994. Large-scale coaggregation of fluorescent lipid probes with cell surface proteins. *J. Cell Biol.* 125:795–802.
Tran, D., J.L. Carpentier, F. Sawano, P. Gorden, and L. Orci. 1987. Ligands internalized through coated or noncoated invaginations follow a common intracellular pathway. *Proc. Natl. Acad. Sci. USA.* 84:7957–7961.
Varma, R., and S. Mayor. 1998. GPI-anchored proteins are organized in submicron domains at the cell surface. *Nature.* 394:798–801.
Yamashiro, D.J., L.A. Borden, and F.R. Maxfield. 1989. Kinetics of α_2-macroglobulin endocytosis and degradation in mutant and wild-type Chinese hamster ovary cells. *J. Cell. Physiol.* 139:377–382.
Yamashiro, D.J., B. Tycko, S.R. Fluss, and F.R. Maxfield. 1984. Segregation of transferrin to a mildly acidic (pH 6.5) para-Golgi compartment in the recycling pathway. *Cell.* 37:789–800.
Yeagle, P.L. 1985. Cholesterol and the cell membrane. *Biochim. Biophys. Acta.* 822:267–287.